https://doi.org/10.46813/2026-164-106

REFINING OF ZIRCONIUM FROM OXYGEN BY ELECTRON BEAM MELTING VIA THE Al_2O SUBOXIDE MECHANISM AND PROSPECTS FOR ADDITIVE MANUFACTURING OF ZIRCONIUM ALLOYS

T.B. Yanko[1], M.M. Pylypenko[2]
[1]UNDERSLAB Ltd, Burgas, Bulgaria;
[2]National Science Center "Kharkiv Institute of Physics and Technology", Kharkiv, Ukraine
E-mail: titanlab3@ukr.net; mpylypenko@kipt.kharkov.ua

The aim of this work was to develop and substantiate a technology for refining zirconium from oxygen during electron-beam melting (EBM) through the formation and removal of volatile Al_2O suboxide, and to investigate the efficiency of alloying zirconium with aluminum during magnesiothermic reduction. Thermodynamic conditions for the reaction $2Al + [O]_{Zr} \rightarrow Al_2O(g)$ at $T > 2000$ °C and residual pressure $\leq 10^{-3}$ Pa are substantiated. Sponge zirconium alloyed with aluminium was produced via magnesiothermic reduction. X-ray diffraction analysis (DRON-3.0 diffractometer, CuKα radiation) identified phases Zr_2Al, Zr_3Al, and Zr_4Al_3. Double-pass EBM refining was performed on the Zr-Al alloy. It was established that after two EBM passes, the oxygen content decreased from 2300 ppm in the as-reduced Zr-Al sponge to 740 ppm, which falls within the target range of 800...1200 ppm specified for nuclear-grade zirconium according to ASTM B350. The residual aluminum content after refining was 0.18 wt.%. Prospects for additive manufacturing technologies (WAAM, SLM) and biomedical applications of zirconium alloys are analysed.

PACS: 81.05.Bx, 81.20.-n, 81.40.-z, 81.65.-b, 61.05.cp, 28.41.-i

INTRODUCTION

Zirconium and its alloys are strategic structural materials for nuclear power engineering due to their uniquely low thermal neutron absorption cross section ($\sigma = 0.18$ barns) and exceptional corrosion resistance in hot water coolant environments. These properties determine the predominant use of Zircaloy-2, Zircaloy-4, M5, and E110 alloys as cladding materials for fuel elements in WWER, PWR, and BWR reactors [1, 2].

Ukraine is among the European countries with the largest number of nuclear power units, which creates a strategic need for domestic production of zirconium and zirconium alloys. The development of a complete technological cycle for nuclear-grade zirconium production – from processing zircon concentrates to manufacturing semi-finished products – is therefore of great importance for the country's energy security.

Ukraine possesses a significant zirconium mineral resource base. The main zirconium ore deposits are associated with placer titanium–zirconium sands, particularly the Malyshivske (Samotkanske), Irshanske, and other deposits. One of the key enterprises is the Vilnohirsk Mining and Metallurgical Combine, where ilmenite–rutile–zircon sands are mined and beneficiated, and zircon concentrate is produced [3].

Control of oxygen content is one of the key technological challenges in the production of nuclear-grade zirconium. Oxygen is an effective interstitial strengthening element, and its concentration directly determines the balance between strength and ductility of the alloy. At the same time, the high thermodynamic stability of oxide phases in the Zr-O system significantly complicates oxygen removal during the refining stage [4, 5]. The proposed refining mechanism, based on the formation and evaporation of volatile Al_2O suboxide during electron-beam melting (EBM), represents a promising approach to addressing this problem [6].

In addition to the nuclear industry, zirconium alloys are increasingly used in medicine, which imposes additional requirements on the quality and purity of the metal [7, 8]. New possibilities for manufacturing zirconium products are opened by additive manufacturing technologies, in particular, Wire Arc Additive Manufacturing (WAAM) and powder-based methods such as SLM and EBM [9, 10].

The aim of this work is to systematize approaches to:

(i) refining zirconium from oxygen during EBM via the formation of Al_2O suboxide;

(ii) a retrospective analysis of domestic zirconium technologies;

(iii) the introduction of aluminum into the alloy, and

(iv) additive manufacturing of zirconium products.

1. INITIAL OXYGEN CONTENT, REGULATORY REQUIREMENTS, AND THERMODYNAMIC FUNDAMENTALS OF REFINING

1.1. INITIAL OXYGEN CONTENT IN ZIRCONIUM REDUCTION PRODUCTS

The oxygen content in zirconium at the stage of primary metal production strongly depends on the reduction process used and the conditions under which it is carried out. The calciothermic zirconium powder (PZrC), produced at the State Research and Production Enterprise "Zirconium", contained oxygen in the range of 2000...6000 ppm, depending on the degree of process optimization [11, 12]. Optimization of calciothermic reduction in a $CaCl_2$ flux melt allows the oxygen content in the powder to be reduced to below 800 ppm, although such a regime requires strict control of technological parameters and is not always maintained in industrial practice [13]. The initial oxygen content in zirconium, depending on the production method, is given in Table 1.

Zirconium sponge produced by magnesiothermic reduction (the Kroll process) contains oxygen in the range of 600...1200 ppm as a result of the lower oxidizing potential of the process compared with calciothermic reduction [12]. Iodide zirconium (Van Arkel-de Boer process), which is used for reference samples and experimental batches, has an oxygen content of ≤100 ppm; however, its production is extremely expensive and not scalable.

The behavior of oxygen during conventional electron-beam melting without a getter is of fundamental importance. As established in [6], gaseous impurities such as hydrogen are removed by degassing from the molten pool, whereas oxygen and nitrogen are practically not removed. A slight decrease in their concentration is compensated by the simultaneous evaporation of zirconium from the melt, and the equilibrium oxygen content remains almost unchanged. This makes conventional vacuum EBM ineffective as a deoxidation method and renders the introduction of a chemical getter – aluminum – the only practical solution.

Table 1

Initial oxygen content in zirconium as a function of the production method

Method of production / material	Oxygen content before refining, ppm	Note
Calciothermic reduction (PZrC), standard conditions	2000...6000	SRPE "Zirconium" [12]
Calciothermic reduction, optimized mode in $CaCl_2$	< 800	Laboratory conditions [13]
Zirconium sponge, magnesiothermic reduction (Kroll process)	600...1200	Titanium Institute [14]
Iodide zirconium (Van Arkel-de Boer process)	≤ 100	Experimental batches [12]
Technological (secondary) Zr after EBM without getter	unchanged	O is not deleted [12]

1.2. REGULATORY REQUIREMENTS FOR OXYGEN CONTENT IN NUCLEAR-GRADE ZIRCONIUM

The ASTM B349 standard for nuclear-grade zirconium (grade R60001) establishes a maximum allowable oxygen content of 1400 ppm (0.14 wt.%). However, the practical requirements of modern reactor designs are more stringent. For alloys such as ZIRLO (Zr-Nb-Sn-Fe) and the domestic alloy E110 (Zr-1%Nb), the optimal target oxygen range is 800...1200 ppm [4]. Within this range, the best balance is achieved between yield strength (~500...600 MPa), ductility (δ = 15...25%), and corrosion resistance under fuel cladding operating conditions. The lower limit of 800 ppm is determined by the requirement to ensure sufficient strength of fuel cladding during accident conditions.

1.3. THE Zr-O SYSTEM AND OXYGEN REMOVAL CHALLENGES

The phase diagram of the Zr-O system is characterized by a wide region of oxygen solid solution in α-Zr (up to ~29 at.% O) and the formation of the stable oxide ZrO_2 [15] (Fig. 1). The standard enthalpy of formation $\Delta H^o(ZrO_2)$ = -1097 kJ/mol is among the highest for metal oxides, which makes oxygen removal by simple vacuum degassing impossible. Moreover, according to [4, 16, 17], the volatility of Al_2O_3 is significantly lower than that of liquid zirconium; therefore, the stable Al_2O_3 formed in the melt cannot be removed by distillation. The only thermodynamically feasible gas-phase pathway is the formation of volatile metal suboxides before oxygen has time to form a stable oxide.

1.4. THERMODYNAMICS OF Al_2O SUBOXIDE FORMATION AND REFINING MECHANISM

Aluminum suboxide Al_2O is a metastable gaseous compound [18] formed by the interaction of liquid Al with oxygen dissolved in zirconium:

$$2\,Al_{(liq)} + [O]_{Zr} \rightarrow Al_2O_{(g)}.$$

The standard Gibbs free energy of formation of $Al_2O(g)$ in the temperature range 2000...2600 K can be approximated by

$$\Delta G^\circ\,(T) = -320000 + 92T \text{ J/mol},$$

$$\Delta G^\circ\,(T) = -1097 \text{ kJ/mol}.$$

Direct removal of oxygen by vacuum evaporation is impossible due to the extremely high stability of ZrO_2. The Al_2O suboxide mechanism bypasses this limitation by forming a volatile intermediate compound.

At temperatures above 2000 °C the Gibbs free energy becomes negative, which thermodynamically enables the formation and evaporation of $Al_2O(g)$ under high-vacuum conditions typical for electron beam melting.

Change in the Gibbs energy of the system taking into account the activities of the components:

$$\Delta G = \Delta G^\circ + RT \ln(p_{Al_2O} / a^2_{Al} \cdot a_{[O]}),$$

where p_{Al_2O} is the partial pressure of the suboxide above the melt, a_{Al} and $a_{[O]}$ are the activities of aluminum and oxygen in the zirconium melt. At T > 2000 °C and the residual pressure in the EBM chamber below 10^{-3} Pa, the condition $p_{Al_2O} < p_{level}$ is fulfilled, and the suboxide is continuously removed from the reaction zone – the process becomes irreversible [6].

According to the Ellingham diagram, aluminum has a significantly higher oxygen affinity than zirconium, which enables oxygen transfer from dissolved Zr-O solution to aluminum with formation of volatile Al_2O species.

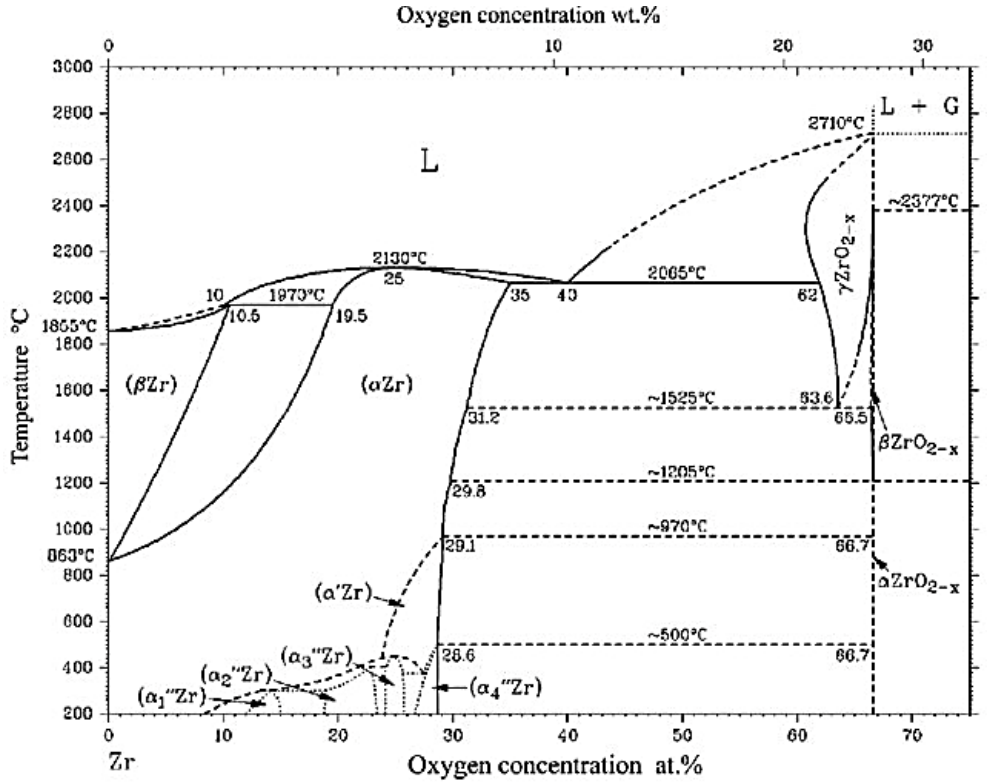

Fig. 1. Zr-O phase diagram [15]

1.5. INFLUENCE OF OXYGEN ON THE MECHANICAL PROPERTIES OF ZIRCONIUM

The mechanism of oxygen strengthening is due to the interaction of dislocations with O atoms in the octahedral interstitial positions of the α-Zr HS lattice. As shown by ab initio methods [19, 20], a strong repulsion occurs between the dislocation and the oxygen atoms in the dislocation core, which leads to transverse sliding and the formation of kinks. Dependence of the yield point:

$$\sigma_y = \sigma_0 + k \cdot C_O^{(1/2)},$$

where $\sigma_0 \approx 100$ MPa, $k \approx 10$ MPa·ppm$^{(-1/2)}$, C_O – O concentration in ppm [21].

Mechanical properties of Zr depending on oxygen content (according to [1, 2, 22]) is given in Table 2.

Table 2

Mechanical properties of zirconium depending on oxygen content and compliance with nuclear standards

Content O, ppm	σ_y, MPa	δ, %	KCU, J/cm²	Nuclear grade compliance
100	≈ 300	38...42	120...140	Too soft for fuel elements
500	≈ 480	25...30	60...80	Lower tolerance limit
800...1200	≈ 550...620	17...25	25...50	Target range (ZIRLO, E110) [1]
≤ 1400	≈ 650...700	12...16	15...25	Maximum per ASTM B349
> 1400	> 700	< 12	< 15	Abnormal, fragility

2. MATERIALS AND METHODS

2.1. SOURCE MATERIALS

In this study, two types of zirconium sponge were used: unalloyed (obtained by magnesiothermic reduction of $ZrCl_4$ according to the standard technology of the Titanium Institute) and aluminum-alloyed (produced using the developed technology for introducing Al during the magnesiothermic reduction process [23]). The initial oxygen content in the unalloyed zirconium sponge was 2600 ppm, while in the Zr–Al-alloyed sponge it was 2300 ppm. The aluminum content in the alloyed sponge was 0.00...2.78 wt.%.

2.2. ELECTRON BEAM MELTING (EBM)

EBM was carried out on the installation of the National Science Center "Kharkiv Institute of Physics and Technology" (Kharkiv) under the following conditions: residual pressure in the chamber 10^{-3}...10^{-4} Pa; melt temperature 2200...2400 °C; duration of exposure of the liquid bath 15...20 min per cycle. For unalloyed zirconium, one EBM cycle was carried out; for the Zr–Al alloy, two consecutive cycles (2 × EBM). Ingots weighing 150...200 g were remelted in a water-cooled copper crystallizer.

2.3. ANALYSIS METHODS

The oxygen, nitrogen, and carbon content were determined by the method of reductive melting in an inert carrier gas (instrumental gas analysis). The chlorine content was determined by potentiometric titration. The aluminum content was determined by atomic absorption spectrometry. X-ray phase analysis (XPA) was performed on a DRON-3.0 diffractometer with automatic software control in monochromated CuKα radiation (λ = 0.15406 nm) at angles 2θ = 20...80°; scan step 0.02°; accumulation time 1 s/step. Phase identification was carried out using JCPDS/ICDD cards. The microstructure was examined under a metallographic microscope at a magnification of ×500 after electrolytic etching.

3. ELECTRON-BEAM MELTING REFINING FROM OXYGEN VIA THE Al_2O SUBOXIDE

3.1. GENERAL PRINCIPLES AND ACHIEVABLE LEVEL OF DEOXIDATION

Electron beam melting (EBM) combines conditions of ultra-high vacuum (residual pressure of 10^{-3}...10^{-4} Pa) with very high melt temperatures (2200...2600 °C), which are necessary for the realization of the suboxide mechanism [12].

The refining task can be formulated as reducing the oxygen content from the 1200...1600 ppm range to the target range of 800...1200 ppm during a single electron-beam melting cycle using an aluminum-based getter. If further adjustment of the composition is required, repeated EBM processing can reduce the oxygen content to below 500 ppm. The degree of oxygen removal is determined by several key factors, including the initial oxygen concentration, the amount of aluminum introduced, the melt temperature, and the duration of the refining process.

The optimal stoichiometry of aluminum addition is calculated from the condition of complete binding of excess oxygen:

$$m_{Al}=2\cdot(M_{Al}/M_O)\cdot(C_{O,init}-C_{O,fin})\cdot m_{Zr}\cdot\eta^{-1},$$

where M_{Al}=26.98, M_O=16.00 g/mol, $C_{O,init}$ and $C_{O,fin}$ are the initial and final oxygen contents (mass fractions), m_{Zr} is the mass of the metal, and η is the thermodynamic yield of the reaction $\eta \approx 0.7...0.85$.

3.2. CONTROL OF RESIDUAL ALUMINUM

A critical limitation is the need for precise control of the amount of aluminum introduced. According to [12], the degree of aluminum removal from liquid zirconium during EBM is only about ~55%, meaning that a significant portion of Al remains in the ingot. Residual aluminum may form the intermetallic compound Al_3Zr or remain in solid solution, which negatively affects corrosion resistance in water environments – an essential property for nuclear applications.

Therefore, for nuclear-grade zirconium, the amount of aluminum added must strictly correspond to the stoichiometric requirement without excess, and the possibility of complete removal of Al in the form of Al_2O must be ensured by appropriate vacuum conditions and sufficient holding time of the melt.

3.3. ALUMINUM INTRODUCTION INTO ZIRCONIUM

The conventional method of introducing metallic aluminum into a consumable electrode is inefficient due to the significant difference in melting temperatures between aluminum and zirconium. As a result, substantial aluminum losses are expected during vacuum melting.

To address this problem, a technology for alloying zirconium with aluminum during the magnesiothermic reduction process was developed. Using this approach, zirconium samples with varying aluminum contents were obtained [23].

The comparison of the microstructures of aluminum-alloyed zirconium sponge and unalloyed zirconium sponge (Fig. 2) confirmed the uniform incorporation of alloying elements into the zirconium matrix, as evidenced by the formation of a microstructure characteristic of zirconium alloys. The microstructure of the unalloyed zirconium sponge consisted of polyhedral grains of the α-phase, with pores located between them (see Fig. 2,a).

In contrast, the microstructure of the aluminum-alloyed zirconium sponge exhibited a clearly defined two-phase structure (see Fig. 2,b), close to a dendritic type. No isolated inclusions were observed in the structure of the zirconium sponge, while the alloying element aluminum is incorporated into the zirconium metallic lattice through the formation of intermetallic sites. The structural constituents of the alloyed zirconium sponge were distributed uniformly throughout the entire volume of the sample investigated, indicating a sufficiently uniform distribution of the alloying element in the zirconium structure. Such a structure is typical for zirconium-aluminum alloys.

X-ray phase analysis of the samples was carried out using a DRON-3.0 diffractometer (measurement conditions are given in Section 2.3). The X-ray diffraction pattern of the aluminum-alloyed zirconium sponge sample is shown in Fig. 3.

X-ray diffraction analysis shows that the main peaks correspond to the B82 structure, characteristic of the Zr_2Al phase, while the secondary peaks correspond to α-Zr, the $L1_2$ structure characteristic of the Zr_3Al phase, and the equilibrium Zr_4Al_3 phase.

The conducted microstructural investigations made it possible to establish that the developed technology enables the production of zirconium sponge with uniform penetration of alloying elements (aluminum) into the zirconium matrix due to the formation of zirconium-aluminum intermetallic compounds.

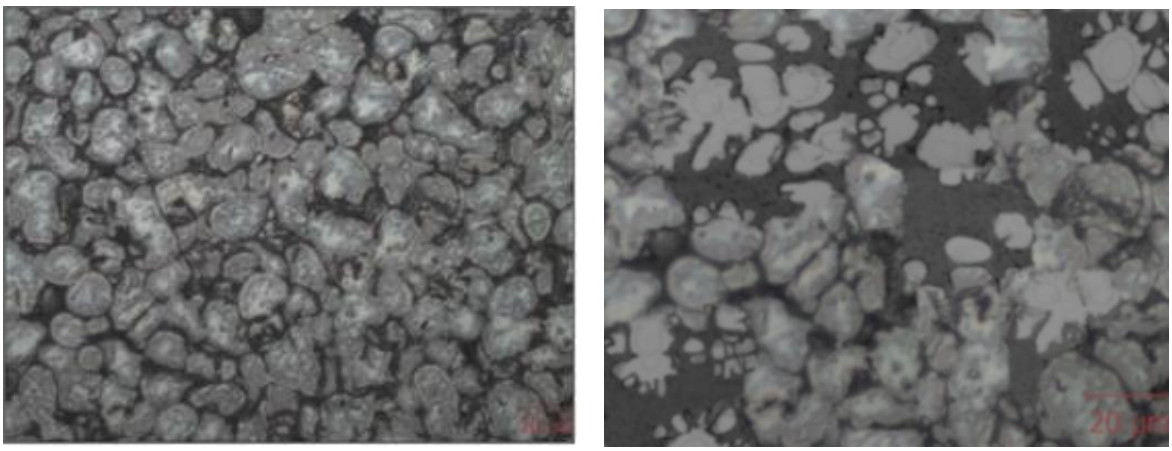

a *b*

Fig. 2. Microstructure of doped and undoped zirconium sponge, x500:
a – undoped zirconium sponge; b – aluminum-doped zirconium sponge

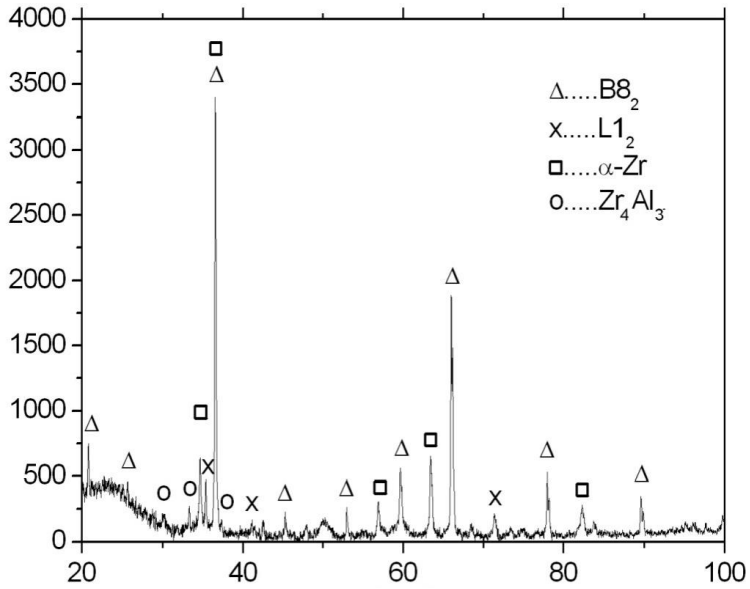

Fig. 3. X-ray diffraction pattern of the aluminum-alloyed zirconium sponge sample

Based on chemical analysis, it has been demonstrated that the developed technology allows achieving the content of the main alloying component (Al) that satisfies the chemical composition requirements of the zirconium-aluminum master alloy according to TU 48-4-453-84.

Studies on electron beam melting of zirconium sponge have demonstrated that oxygen content decreases even after a single EBM process without a getter (from 2600 to 2100 ppm). However, this reduction remains limited and is primarily attributed to the removal of moisture and adsorbed oxygen, while significant deoxidation occurs only with the introduction of an Al-based getter (Table 3). After double EBM of the Zr-Al alloy, the oxygen content decreased from 2300 to 740 ppm, falling below the target nuclear-grade range of 800...1200 ppm specified in ASTM B350.

Table 3

Compositions of the studied zirconium alloys for deoxidation

Material	Content of impurities and alloying elements, ppm				
	Cl	N	C	Al, wt.%	O
Zirconium sponge	210	200	230	–	2600
Zirconium after EBM	3.1	0.006	120	–	2100
Zirconium-Aluminum sponge	280	340	220	2.78	2300
Zirconium-Aluminum alloy after 2 × EBM	3.6	0.006	130	0.18	740

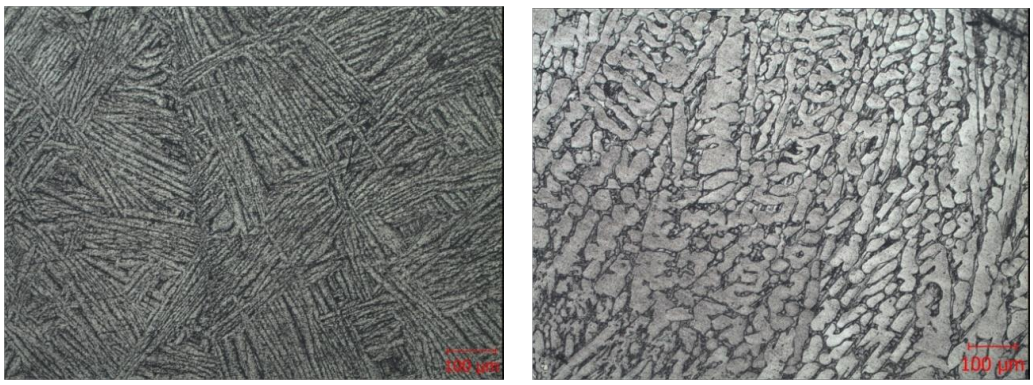

a *b*

Fig. 4. Microstructures of zirconium and zirconium–aluminum alloy after melting

The aluminum content after refining was 0.18 wt.%, which exceeds the ASTM B350 limit (≤ 0.0075 wt.%) and therefore requires either an additional EBM cycle or optimization of the amount of introduced aluminum. At the same time, with respect to other metallic impurities, the obtained metal satisfies the ASTM B350 requirements.

As shown in Fig. 4, zirconium after melting exhibits a lamellar basket-weave microstructure. The lamellae are arranged in packets and oriented at specific angles relative to one another. A well-defined α-phase is observed in the form of individual light grains. Dark regions are visible along the grain boundaries, corresponding to impurity inclusions.

In contrast to pure zirconium, the zirconium–aluminum alloy exhibits a well-defined two-phase microstructure. A pronounced dendritic morphology of the α-phase is observed, in which primary and secondary dendrites, as well as, to a lesser extent, tertiary dendrites, can be distinguished. In the interdendritic regions, a second, darker phase of eutectoid origin is observed.

Thus, the microstructure of the experimental zirconium–aluminum alloys is homogeneous, with a uniform distribution of alloying elements within the zirconium matrix.

The industrial implementation of the developed zirconium alloying technology would significantly simplify the EBM refining process.

4. ZIRCONIUM ALLOYS IN BIOMEDICAL APPLICATIONS

Zirconium and its alloys satisfy the key requirements for metallic biomaterials, including biocompatibility, corrosion resistance in physiological environments, and the absence of cytotoxicity. The elastic modulus of zirconium alloys (88...99 GPa) is significantly closer to that of cortical bone than to that of stainless steel (≈200 GPa) or Co-Cr alloys (200...230 GPa), thereby substantially reducing the stress-shielding effect during implantation [10].

The lower magnetic susceptibility of Zr compared to Ti-6Al-4V represents a significant advantage for patients undergoing magnetic resonance imaging (MRI) [7].

Wear resistance is a critical property of joint endoprosthetic components. Thermal oxidation of zirconium implants at 500...530 °C in a controlled atmosphere results in the formation of a ZrO_2 layer 5...20 μm thick, with a hardness exceeding 10 GPa and wear resistance an order of magnitude higher than that of the base metal [8]. This technology underpins commercially available oxidized zirconium–niobium implants (Oxinium™). The microstructure and properties of the oxide layer are directly depend on the oxygen content in the base metal, a parameter controlled during the EBM refining stage.

5. WAAM AND POWDER TECHNOLOGIES FOR ZIRCONIUM ALLOYS

The production of zirconium alloys with low oxygen and impurity contents enables the broader development of additive manufacturing technologies for zirconium components [10]. Wire Arc Additive Manufacturing (WAAM) is the most cost-effective method for producing large components from wire feedstock, with deposition rates reaching 4...9 kg/h, significantly exceeding the productivity of powder-based technologies such as selective laser melting (SLM) and EBM [9,10].

The application of WAAM to zirconium alloys requires a protective atmosphere (vacuum or argon with a purity of ≥99.998%), while the tendency to form a columnar grain structure necessitates optimization of the thermal cycle.

Plasma atomization of zirconium wire (PAW) is the most widely used method for producing spherical powders for SLM/EBM, with particle sizes in the range of 15...150 μm.

Comparison of additive manufacturing methods for zirconium products is given in Table 4.

6. CLOSED TECHNOLOGICAL CHAIN

The combination of zirconium alloying during magnesiothermic reduction, electron-beam melting (EBM) refining and additive manufacturing technologies makes it possible to establish a closed technological cycle:

1. Production of zirconium sponge by the magnesiothermic method, followed by controlled alloying with aluminum.

2. EBM refining from oxygen via the Al_2O suboxide mechanism at $T > 2000$ °C and $p \leq 10^{-3}$ Pa, achieving the target oxygen content in the range of 800...1200 ppm for nuclear alloys (ASTM B350).

3. Plasma atomization of wire can be employed to obtain spherical powders (for SLM and EBM), or direct

fabrication of components can be achieved using WAAM for civil, medical, or nuclear applications.

The proposed technological chain minimizes the number of remelting operations, preserves the achieved level of metal purity, and provides flexibility in selecting the final manufacturing method depending on the intended application.

Table 4

Comparison of additive manufacturing methods for zirconium products

Method	Source material	Resolution, mm	Productivity	Main limitations
SLM/LBM*	Powder 15...45 μm	0.1...0.2	Up to 1000 g/h	Inert atmosphere, powder cost
EBM (PBF**)	Powder 45...105 μm	0.2...0.5	Up to 5000 g/h	Vacuum; porosity
WAAM	Wire Ø 1...3 mm	1...5	Up to 4...20 kg/h	Roughness; columnar structure

*LBM – Laser Beam Melting; **PBF – Powder Bed Fusion.

CONCLUSIONS

A technology for alloying zirconium with aluminum during magnesiothermic production has been developed. X-ray phase analysis confirmed the formation of intermetallic phases Zr_2Al, Zr_3Al, and Zr_4Al_3 in the zirconium sponge, indicating uniform distribution of the alloying element.

The thermodynamic mechanism of zirconium refining from oxygen during EBM through the formation and removal of Al_2O(g) at T > 2000 °C and $p \leq 10^{-3}$ Pa has been substantiated. It was shown that the initial calciothermic powder (PZrC) contains 2000...6000 ppm O, and that the Al_2O mechanism (confirmed for the titanium analogue, with reduction to 100...500 ppm [22]) enables achieving the target nuclear-grade range of 800...1200 ppm in a single EBM cycle. Conventional EBM without a getter is ineffective for oxygen removal [13]. Experimental results confirm that double EBM of the Zr-Al alloy reduces the oxygen content from 2300 to 740 ppm (see Table 3). The amount of introduced aluminum requires precise control, since excess aluminum (with a removal degree of ~55% [13]) leads to contamination of the refined ingot with the Al_3Zr phase, which is unacceptable for nuclear-grade zirconium.

Based on the analysis of publications [7, 8], the prospects of zirconium alloys in medical applications have been demonstrated. An oxidized ZrO_2 surface provides wear resistance an order of magnitude higher than that of Ti-6Al-4V, while the oxygen content in the base metal is a critical parameter determining implant quality.

The prospects of WAAM and SLM technologies for manufacturing zirconium components with complex geometries, including personalized porous medical implants, have been analyzed.

A closed technological chain concept has been formulated: alloyed zirconium sponge → EBM refining → additive manufacturing, representing a production sequence that minimizes gas contamination of the metal.

REFERENCES

1. B.O. Okonkwo, Z. Li, L. Li, et al. Research progress on zirconium alloys: applications, development trend, and degradation mechanism in nuclear environment // *Corrosion Reviews.* 2024, N 6, p. 609-628; https://doi.org/10.1515/corrrev-2024-0075

2. G. Sukhomlin, T. Dergach. Features of formation of structure and properties of Zr-1Nb alloy when manufacturing fuel element shell tubes // *Science Rise.* 2019, N 12(65), p. 10-15; https://doi.org/10.15587/2313-8416.2019.189283

3. L.V. Shpylovyi, V.S. Biletskyi. Ukrainskyi tsyrkonii [Ukrainian zirconium] // *Zbahachennia Korysnykh Kopalyn.* 2019, N 73(114), p. 41-55 (in Ukrainian); https://doi.org/10.13140/RG.2.2.23748.78728

4. K. Vutova, V. Stefanova, E. Manoilov, et al. The Impact of Electron Beam Melting on the Purification of Recycled Zirconium // *Metals*. 2025, N 15(11), p. 1273; https://doi.org/10.3390/met15111273

5. S.V. Ladokhin, V.S. Vakhrusheva. Application of electron beam melting for producing zirconium alloys in Ukraine // *Electrometallurgy Today.* 2018, N 4, p. 36-41; https://doi.org/10.15407/sem2018.04.02

6. V.M. Azhazha, P.N. Vyugov, S.D. Lavrinenko, et al. Electron beam melting of titanium, zirconium and hafnium // *Proceedings of the XV International Conference on Physics of Radiation Phenomena and Radiation Materials Science*. 2002, p. 10-15.

7. A. Mehjabeen, T. Song, W. Xu, et al. Zirconium Alloys for Orthopaedic and Dental Applications // *Advanced Engineering Materials.* 2018, v. 20, N 9, art. 1800207; https://doi.org/10.1002/adem.201800207

8. J.-W. Ge, W.-Z. Han. Friction and Wear Behaviors of Oxygen-Charged Zirconium // *Advanced Engineering Materials.* 2025, v. 27, N 21, art. 2501018; https://doi.org/10.1002/adem.202501018

9. T.A. Rodrigues, V. Duarte, R.M. Miranda, et al. Current Status and Perspectives on Wire and Arc Additive Manufacturing (WAAM) // *Materials*. 2019, v. 12, N 7, p. 2-42, art. 1121; https://doi.org/10.3390/ma12071121

10. S.L. Schwab, R.V. Selin, M.M. Voron, et al. Microstructure of the Ti-Zr-Nb system alloy obtained by the WAAM method with a metal powder wire // *Suchasna Elektrometalurhiya*. 2025, N 1, p. 51-57 (in Ukrainian); https://doi.org/10.37434/sem2025.01.09

11. V.M. Azhazha, P.N. Vyugov, S.D. Lavrinenko, M.M. Pylypenko. Purification of calcium-thermal zirconium and hafnium from oxygen // *Problems of Atomic Science and Technology.* 1997, N 1(65), 2(66), p. 144-145.

12. V.M. Azhazha, P.N. Vyugov, S.D. Lavrinenko, et al. *Zirconium and its alloys: production technology and fields of application*. Kharkiv: "NSC KIPT", 1998, 89 p.

13. A.M. Abdelkader, E. El-Kashif. Calciothermic reduction of zirconium oxide in molten $CaCl_2$ // *ISIJ International.* 2007, N 47(1), p. 25-31;
https://doi.org/10.2355/isijinternational.47.25

14. Patent 82174 Ukraine, МПК51 C22B34/14. *The device for magnesium-thermal reduction of zirconium tetrachloride* / O.P. Yatsenko, O.D. Sushchynskyi, R.A. Shcherban, T.B. Yanko, S.D. Lavrynenko, M.M. Pylypenko. Published 25.07.2013, Bul. № 14.

15. H. Okamoto. O-Zr (Oxygen-Zirconium) // *Journal of Phase Equilibria and Diffusion.* 2007, N 28 (5), p. 498-498;
https://doi.org/10.1007/s11669-007-9154-2

16. E. Copland. Comparing the Thermodynamic Behaviour of Al(l) + ZrO_2 (4% Y_2O_3) and Al(l) + Al_2O_3 // *International Journal of Materials Research.* 2006, N 97(8), p. 1108-1114;
https://doi.org/10.1515/ijmr-2006-0174

17. L.A.T. Pereira, L.G. Martinez, C.S. Mucsi, et al. On the melting of zirconium alloys from scraps using electron beam and induction furnaces – recycling process viability // *Journal of Materials Research and Technology.* 2020, v. 9, N 3, p. 4867-4875;
https://doi.org/10.1016/j.jmrt.2020.03.006

18. M. Hoch, H.L. Johnston. Formation, Stability and Crystal Structure of the Solid Aluminum Suboxides: Al_2O and AlO // *J. Am. Chem. Soc.* 1954, v. 76, p. 2560-2561; DOI: 10.1021/ja01638a076

19. E. Kautz, B. Gwalani, Z. Yu, et al. Investigating zirconium alloy corrosion with advanced experimental techniques: a review // *Journal of Nuclear Materials.* 2023, v. 585, p. 154586;
https://doi.org/10.1016/j.jnucmat.2023.154586

20. U. Stoll, N. Slavinskaya. Corrosion behavior of zirconium alloys in the aqueous environment. Phenomenological aspects. Overview // *Journal of Nuclear Science and Technology.* 2023, v. 60, N 5, p. 573-602;
https://doi.org/10.1080/00223131.2022.2127954

21. N. Chaari, D. Rodney, E. Clouet. Oxygen – Dislocation interaction in zirconium from first principles // *Acta Materialia*. 2017, v. 132, p. 416-424;
https://doi.org/10.1016/j.actamat.2017.05.008

22. V. Trush, M. Pylypenko, P. Stoev, et al. Influence of interstitial elements (oxygen, nitrogen) on properties of zirconium alloys (review) // *Physics and Chemistry of Solid State.* 2022, v. 23, N 2, p. 401-415;
https://doi.org/10.15330/pcss.23.2.401-415

23. T.B. Yanko. *Development of technology for complex alloying of titanium and zirconium during magnesium-thermal reduction:* Abstract of dissertation Ph.D. (Technology) Special 05.16.02. Dnipro: "NMetAU", 2016, 20 p.

Article received 18.05.2026

РАФІНУВАННЯ ЦИРКОНІЮ ВІД КИСНЮ ПРИ ЕЛЕКТРОННО-ПРОМЕНЕВОМУ ПЕРЕПЛАВІ З ВИКОРИСТАННЯМ СУБОКСИДУ АЛЮМІНІЮ Al_2O ТА ПЕРСПЕКТИВИ АДИТИВНОГО ВИРОБНИЦТВА ЦИРКОНІЄВИХ СПЛАВІВ

Т.Б. Янко, М.М. Пилипенко

Метою роботи була розробка та обґрунтування технології рафінування цирконію від кисню при електронно-променевому переплаві (ЕПП) через утворення та видалення леткого субоксиду Al_2O, а також дослідження ефективності легування цирконію алюмінієм у процесі магнієтермічного відновлення. Термодинамічно обґрунтовано умови реакції $2Al + [O]_{Zr} \rightarrow Al_2O(г)$ при T > 2000 °C та залишковому тиску $\leq 10^{-3}$ Па. Отримано зразки губчастого цирконію, легованого алюмінієм, методом магнієтермічного відновлення. Рентгенофазовим аналізом (дифрактометр ДРОН-3.0, CuKα) ідентифіковано фази Zr_2Al, Zr_3Al та Zr_4Al_3. Проведено двократний ЕПП сплаву Zr-Al. Встановлено, що після двократного ЕПП вміст кисню знижується з 2300 ppm (губчастий Zr-Al) до 740 ppm, що відповідає цільовому діапазону ядерного цирконію 800...1200 ppm за ASTM B350. Вміст алюмінію після рафінування становив 0,18 мас.%. Проаналізовано перспективи технологій адитивного виробництва (WAAM, SLM) та біомедичні застосування цирконієвих сплавів.